Materials Today Chemistry 39 (2024) 102155

Contents lists available at ScienceDirect

Materials Today Chemistry

journal homepage: www.journals.elsevier.com/materials-today-chemistry/

Room temperature synthesis of triazine covalent organic frameworks for size-selective intercalation of molecules and fast water purification

Maryam Salahvarzi [a], Antonio Setaro [b,c], Siamak Beyranvand [a], Mohammad Nemati [a], Georgy Gordeev [b], Alphonse Fiebor [b], Kai Ludwig [d], Reza Ghanbari [e], Nima Nasiri [e], Vahid Ahmadi [f], Manuela Weber [g], Zahra Jamshidi [e,h], Chong Cheng [i], Stephanie Reich [b], Mohsen Adeli [a,b,*]

[a] Department of Organic Chemistry, Faculty of Chemistry, Lorestan University, Khorramabad, Iran
[b] Department of Physics, Free University Berlin, Arnimallee 14, 14195, Berlin, Germany
[c] Department of Engineering, Pegaso University, Naples, Italy
[d] Forschungszentrum für Elektronenmikroskopie and Core Facility BioSupraMol, Institut für Chemie und Biochemie, Freie Universität Berlin, Fabeckstr. 36a, 14195 Berlin, Germany
[e] Chemistry Department, Sharif University of Technology, Tehran, 11155-1639, Iran
[f] Institut für Chemie und Biochemie, Freie Universität Berlin, Takustrasse 3, 14195, Berlin, Germany
[g] Department of Chemistry, Biochemistry & Pharmacy, Free University Berlin, Arnimallee 22, 14195, Berlin, Germany
[h] Theoretical Chemistry, Institute of Physical Chemistry, Heidelberg University, Im Neuenheimer Feld 229, 69120, Heidelberg, Germany
[i] College of Polymer Science and Engineering, State Key Laboratory of Polymer Materials Engineering, Sichuan University, Chengdu, 610065, China

ARTICLE INFO

Keywords:
Water purification
Catalyst-free cyclotrimerization
Covalent organic frameworks
Intercalation
Triazine frameworks

ABSTRACT

In this work, we report on a new method for the construction of triazine covalent organic frameworks on gram scale by catalyst-free cyclotrimerization of alkynes at room temperature for the size-selective intercalation of molecules and fast water purification. Reaction between sodium acetylide and cyanuric chloride resulted in 2,4,6-triethynyl-1,3,5-triazine intermediate which converted to heteroaromatic frameworks comprising triazine and benzene rings upon in situ [2 + 2+2] cyclotrimerization. Mechanistic studies revealed a crucial role for the triazine ring in susceptibility of ethynyl groups to cyclization. The permeability of these nanostructures to small molecules, exemplified by Rhodamine 6G (R6G) and $HAuCl_4$, and their impermeability to bigger objects such gold nanoparticles (5 nm) indicated their potential to remove molecular impurities from water. Impurities including Methylene blue and Malachite green with 20 mg L^{-1} concentration were completely removed by 1 mg of the synthesized frameworks in 60 s. Taking advantages of the straightforward synthesis and permeability to small molecules, the synthesized triazine frameworks can be used for the fast and efficient purification of water contaminated by toxic agents.

1. Introduction

Covalent organic frameworks (COFs) with the porous and stable structures have been used for a broad range of applications including water purification and nanofiltration [1], owing to their ability for the efficient loading, intercalation and transportation of small molecules [2,3]. However, scalable, cost-effective and straightforward synthesis of COFs with stable backbones at mild conditions is one of the main challenges that hamper their future applications [4–6]. Carbon-carbon couplings are known reaction pathways for the construction of carbon-based nanomaterials, yet COFs have remained difficult to prepare by this method [7–11]. Among the carbon-carbon couplings, the cyclization of alkynes to the benzene ring has shown great promise for the construction of new materials, due to its versatility [12]. It is usually catalyzed by transition-metal complexes and is a very powerful tool in the arsenal of organic chemists for the construction of benzene derivatives in a one-pot reaction. In this reaction each alkyne molecule forms two new carbon-carbon σ bonds at the expense of one π bond. Over several decades the mechanism of this reaction has been intensively studied [13]. As the core area of interest, two steps have been

* Corresponding author. Department of Organic Chemistry, Faculty of Chemistry, Lorestan University, Khorramabad, Iran.
E-mail address: adeli.m@lu.ac.ir (M. Adeli).

https://doi.org/10.1016/j.mtchem.2024.102155
Received 23 February 2024; Received in revised form 4 June 2024; Accepted 9 June 2024
Available online 13 June 2024

verified for the catalyst action namely, the coordination of the catalyst with the π bonds of two alkyne units and the cyclization of the created metallacyclopentadienes with a further alkyne through intramolecular [4 + 2] cycloaddition or the Schore route [14–19]. Great effort has been devoted to develop different catalysts and to optimize the yield, chemo-, stereo- and regioselectivity of cyclotrimerization of alkynes [18–20]. While understanding the catalyst action has opened new ways for regulating cyclotrimerization of alkynes, other important parameters such as the structural effects of the reagents have been almost ignored. Therefore, the development of [2 + 2+2] cycloaddition to construct organic frameworks has been limited by catalyst efficiency [21–24]. Inapplicability of this well-known reaction to construct COFs postpone scalable production of platforms for size selective screening or intercalation of small molecules. As an alternative, the catalyst-free cyclotrimerization of alkynes under various conditions has been studied and valuable results have been achieved [25]. Regardless of the required co-catalysts and co-reagents, the catalyst-free cyclotrimerization of alkynylketones at relatively low temperatures promised new pathways for the cyclization of alkynes, circumventing the catalyst-dependent limitations and side reactions at high temperatures [26]. The polarization of carbon-carbon triple bonds by adjacent carbonyl groups plays a crucial role in their susceptibility to trimerization [16,27]. Excluding catalyst and performing cyclotrimerization of alkynes at ambient conditions are two important factors for the cost-effective and scalable production of stable COFs by this method. Moreover, it provides a new pathway for the manipulation of the structure of COFs in terms of functionality and pore size that affect their interactions with small molecules such as water impurities [28,29].

In this work, we report on a new method for the construction of heteroaromatic covalent organic frameworks on gram scale by catalyst-free electron deficient [2 + 2+2] cyclotrimerization of alkynes at room temperature for the size-selective intercalation of molecules and fast water treatment. One-pot reaction between sodium acetylide and 2,4,6-trichloro-1,3,5-triazine resulted in highly reactive intermediates that changed to covalent organic frameworks comprising benzene and triazine rings upon in situ cyclotrimerization. Mechanistic studies showed a key role for triazine ring in increasing the reactivity of ethynyl groups toward cyclotrimerization. The constructed covalent organic frameworks were used for the molecular intercalation and water purification. While small molecules, such as R6G and $HAuCl_4$ were able to penetrate into the heteroaromatic covalent organic frameworks intensively, larger objects such as 5 nm gold nanoparticles were not able to pass through the layers. Accordingly, they were used for the removing molecular impurities from water. Sonication of covalent organic frameworks in the contaminated water for 30–60 s followed by centrifugation or immersing a sponge-supported frameworks in these

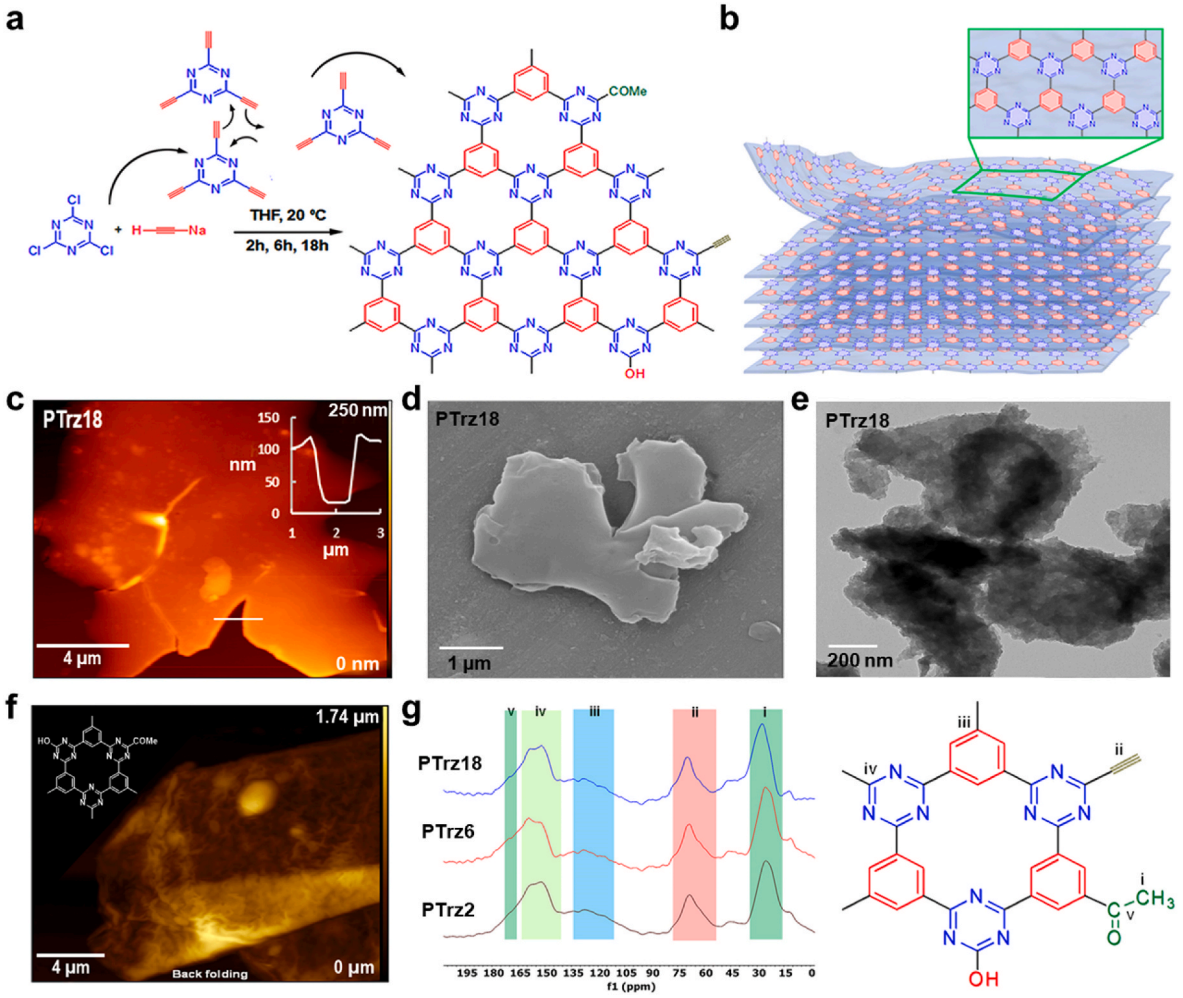

Fig. 1. (a) Schematic representation of the synthesis of porous heteroaromatic frameworks. (b) Lateral growing and vertical stacking of PTrz sheets. (c) Atomic force microscopy (AFM) image of the product of reaction at 18 h. (d) Scanning electron microscopy (SEM) image of PTrz18. (e) Conventional transmission electron microscopy (TEM) image of the product of reaction at 18 h. (f) AFM image of PTrz18, exfoliated in solution, represents back folding that is expected for the two-dimensional materials with big lateral size. (g) ^{13}C CP-MAS-NMR spectra of PTrz with distinguished signals for the triazine and benzene rings as well as ethynyl and methyl ketone functional groups.

solutions resulted in complete removal of dyes including Methylene blue and Malachite green.

2. Results and discussion

Triazine covalent organic frameworks are synthesized by a cost-effective and straightforward reaction including one-pot catalyst-free cyclotrimerization of alkynes at room temperature on gram scale (Fig. 1a).

The nucleophilic substitution of chlorine atoms of cyanuric chloride by sodium acetylide resulted in reactive intermediates comprising a triazine core and ethynyl groups that changed to polytriazine frameworks (PTrz) upon cyclotrimerization (movie 1).

The growth of the sheets was monitored by performing the reaction at three different time frames. Fig. 1c and S2shows AFM images of products of 2 h, 6 h and 18 h reactions which were labeled as PTrz2, PTrz6 and PTrz18, respectively. The product of the 2 h reaction consisted of inhomogeneous flat materials laterally connected with bigger sheets (Fig. S2c). After 6 h, sheet-like structures with clear edges in the micrometer range were formed. Small particles joining the edges of the big sheets was counted for their lateral growth (Fig. S2d). After 18 h, the product contained sheet-like structures with several micrometers lateral size and clear edges (Fig. 1c and f). The thickness and basal plane of the material increased simultaneously with increasing the reaction time, pointing towards concurrent lateral and vertical growth. Lateral cross-linking and vertical growth of the materials correspond to the cyclotrimerization of ethynyl groups and π-π stacking of their backbone (Fig. 1b). In some cases, big holes with few hundred nanometers diameter and ~30 nm depth on the basal plan of PTrz18 were observed (Fig. S2a). These holes were assigned to the mismatched lateral cross-linking of small sheets during the formation of sublayers and driving the growth of upper layers to the same topology by π-π interactions. This is similar to the lateral growth of boronic acid derived covalent organic frameworks [30–32]. However, in this case, the reaction is irreversible to heal the defects by dynamic cleavage and bond formation.

The noncovalent interactions between the PTrz18 layers were confirmed by scotch tape exfoliation to few layers (Fig. S2b). The results of AFM experiments were confirmed by SEM and TEM images, where a clear trend from irregular materials towards big sheets with progressing reaction time was observed (Fig. 1d and e, S3a, S3b and S4).

While PTrz2 did not show any clear morphology, the product of the 18 h reaction contained integrated sheet-like structures with several micrometer lateral size and observable folds (Fig. 1f). Small particles attached to the periphery of big cores conformed the lateral growth of PTrz (Fig. S4).

Thanks to the water dispersibility of PTrz18, the morphology of this compound was investigated by Cryo-TEM and Cryo-electron tomography (cryo-ET) (Fig. S1). In agreement with the AFM and conventional TEM images, cryo-ET showed a sheet-like structure for this compound (Movie 2). Tomograms (Fig. S1b and movies 1 and 2) revealed that PTrz18 consists of many stacked layers with ~100 nm thickness. Accordingly, the SEM images showed a flat morphology for PTrz6 and PTrz18. The segregated structure of PTrz2 and unified structures of PTrz6 and PTrz18 indicated the integration of the backbone of these materials over time (Fig. 1d and S3b).

The structure of PTrz was investigated by ^{13}C solid-state cross-polarization magic-angle-spinning (CP-MAS) nuclear magnetic resonance (NMR) (Fig. 1g). The NMR spectra of PTrz2, PTrz6 and PTrz18 showed signals at 150–170 ppm and 100–150 ppm that were assigned to the carbon atoms of triazine and benzene rings, respectively [33–35]. The signal of the benzene ring corresponds to the cyclotrimerization of ethynyl groups. The signal at 55–75 ppm was attributed to the unreacted ethynyl groups. The shoulder at 170–180 ppm together with the signal at 30 ppm were assigned to the methyl ketone functional groups (Fig. 1g). The pathway of creating methyl ketone functional groups is discussed in the mechanism section.

The similarity of the NMR spectra of PTrz2, PTrz6 and PTrz18 showed that the main backbone of these materials forms in the first 2 h of reaction. Lengthening the reaction time develops the basal plane and improves the integration through lateral crosslinking.

The IR spectra of the product of different reaction times showed absorbance bands at 1640-1650 cm^{-1} and 1520-1530 cm^{-1} for the stretching vibrations of the carbon-carbon and the carbon-nitrogen double bonds, respectively. A broad absorbance band at 2900-3600 cm^{-1} corresponds to the hydroxyl functional groups of PTrz (Fig. S6a). The formation of these hydroxyl functional groups is discussed in the mechanism section.

The Raman spectra of PTrz6 and PTrz18 showed two broad peaks centered at 1550 cm^{-1} and 1350 cm^{-1} and slightly shifted peaks at 1558 cm^{-1} and 1344 cm^{-1} for PTrz2 (Fig. S6b). The peak at 1550 cm^{-1} showed 30 cm^{-1} downshift compared to the G peak of graphite. This agrees with a shift expected for the heavier nitrogen atoms because the frequency is inversely proportional to the square root of the vibrating atoms. To explore the source of vibrational modes, Raman spectra of small molecules including 2,4,6-trichloro-1,3,5-triazine (Trz), biphenyl (BP), 2-chloro-4,6-diphenyl-1,3,5-triazine (CDT) with a structure similar to the repeating unit of PTrz were recorded (Fig. S5b). BP, as a model for benzene rings, showed C–C–C stretching, bridge C–C stretching, in-plane C–H bending and trigonal breathing modes at 1610 cm^{-1}, 1283 cm^{-1}, 1046 cm^{-1} and 1006 cm^{-1} respectively [36]. 2,4,6-trichloro-1,3,5-triazine (Trz) that was one of the precursors and source of triazine rings showed in-plane ring vibrations at 1505 cm^{-1}, 1264 cm^{-1} and 983 cm^{-1} [37]. 2-chloro-4,6-diphenyl-1,3,5-triazine as a combination of benzene and triazine rings and similar to the repeating unit of PTrz, showed several new Raman modes at 1546 cm^{-1}, 1437 cm^{-1}, 1399 cm^{-1} and 1369 cm^{-1} in addition to the intrinsic modes of cyanuric chloride and biphenyl. While attachment of two benzene rings to triazine resulted in several new vibrational modes, long range combination of these rings in the structure of PTrz should give rise to various Raman modes resulting in broad peaks. Overlapping the new Raman modes, centered at 1558-1350 cm^{-1}, with intrinsic vibrations of triazine and benzene rings resulted in two broad peaks in the Raman spectrum of non-exfoliated PTrz (Fig. S6b). These peaks correspond to the typical D and G modes in the visible Raman spectra of triazine two-dimensional structures [38,39]. After exfoliation, significant changes in the Raman modes of PTrz were observed (Fig. S5a). Peaks at 1572 cm^{-1}, 1415 cm^{-1}, 1310 cm^{-1} and 1174 cm^{-1} in the Raman spectrum of exfoliated PTrz were very similar to the vibrational modes of the functionalized graphene sheets.

The composition of the synthesized materials was studied by elemental and EDX analysis. The carbon/nitrogen (C/N) ratios that indicates the benzene/triazine composition were found to be 1.84, 1.77 and 1.78 for PTrz2h, PTrz6h and PTrz18h respectively (Figs. S5c and S7). The lower carbon content of the synthesized materials in comparison with intermediate or ideal structure (C/N = 2.57) was due to the substitution of some chlorine atoms of cyanuric chloride by oxygen containing functional groups. The P-XRD diffractograms of PTrz2h, PTrz6h and PTrz18h showed the low-angle peak at around 14 2θ belong to the in-plane (100) reflection, while the broad (001) diffraction peak at around 25 2θ can be attributed to the interlayer stacking of sheet-like triazine frameworks. Over time the low angle (100) peak is increased in intensity compared to the interlayer (001) peak, which could point to an enhanced intralayer structuring with ongoing reaction time (Fig. S8) [40,41].

This is supported by AFMresults, where an increase in the thickness of the material with the reaction time was observed. TGA thermograms showed two points of main weight loss for PTrz at 100–350 °C and 350–800 °C corresponding to the detaching of functional groups and the decomposition of their backbone (Fig. S5d). Similar thermal behaviors for the materials with the same repeating units have been before reported [40,42]. Moreover, the more integrated backbone of sheet-like benzene-triazine heteroaromatic structures at longer reaction times

was manifested in the higher thermal stability of PTrz18h.

The mechanism of the reaction between cyanuric chloride and sodium acetylide was investigated by density functional theory and molecular models to acquire more information about the structure of materials and explore the possible reaction pathways (Fig. S5e-g and S13).

Three degenerate bonding and anti-bonding molecular orbitals were obtained by natural bond orbital analysis of the ground state geometry of triethynyl-1,3,5-triazine (Fig. S5e). Localizing the bonding orbitals on the carbon-carbon triple bonds and antibonding orbitals on triazine ring indicated more nucleophilic and electrophilic characteristics for these segments, respectively. Moreover, triple bonds were polarized by electro poor triazine segment and this factor was one of the main reasons for the high reactivity of this compound toward cyclotrimerization (Fig. S5f), as confirmed by experimental data in the following. While the carbon of ethynyl substituents connected to a triazine ring showed an atomic charge of −0.06e, carbons bearing hydrogen atoms were more than two times (−0.131e) negatively charged. The polarization of the triple bonds induced a nucleophilic and electrophilic character for the carbons away from triazine and close to this ring and triggered the cyclotrimerization of triethynyl-1,3,5-triazine and formation of benzene rings. Figs. S5g and S13 and Table S8 display the charge distribution through the relaxed scan of the reaction path of cyclotrimerization. Charge distribution analyses for these steps exhibited decreasing the localized charges of nitrogen atoms of triazine rings and carbons of alkynyl substituents, which is caused by the charge transfer from HOMOs to LUMOs in the three molecules involved in the cyclotrimerization.

Substitution of two chlorine atoms of cyanuric chloride by unreactive groups and confining the reaction at the molecular level were required to study the structure of reaction intermediates. Accordingly, the reaction between 2-chloro-4,6-diphenyl-1,3,5-triazine (**1**) and sodium acetylide was monitored by NMR and mass spectroscopy and the final product was analyzed by single crystal XRD. We recognized **A** and **B** pathways, where **A** yielded the major product 4,6-diphenyl-1,3,5-triazin-2-ol (**5**). A minor product (**3**) as the result of cyclotrimerization was also detected by mass spectroscopy (Fig. 2b). ^{1}H and ^{13}C NMR showed that compound (**5**) is the intermediate of pathway **A** (Fig. 2d and e). The signal at 294 m/z in the mass spectrum of reaction mixture was related to the molar mass of this intermediate accompanied by proton (calculated for $C_{17}H_{15}N_3O_2$ [M+H]: 293.12) (Fig. 2f). The final product of this reaction route was compound (**6**).

Signals of this compound accompanied by proton, sodium and potassium ions can be seen at 250 m/z, 272 m/z, 288 m/z, respectively (calculated for $C_{15}H_{11}N_3O$ [M+H], [M+Na] and [M+K]: 250.1 m/z and 272.08 m/z and 288.05 m/z respectively) (Fig. 2f). Single X-ray crystallography showed a tautomerized form of compound (**6**), where the hydrogen atom shifted to the neighbor nitrogen atom of the triazine ring (Fig. 2c). From this reaction pathway we learned that the conjugation of an ethynyl group to a triazine ring dramatically increases its susceptibility to nucleophilic reactions. Also, we understood that the oxygen containing functional groups including methyl ketone and hydroxyl groups in PTrz are created by this reaction pathway. The amount of the product of pathway **B** was not enough to collect for further analysis but it was detected in the mass spectra of the reaction mixture (Fig. 2b). The lower tendency of the reaction toward pathway **B** can be assigned to either electronic effects or steric hindrance of the phenyl substituents. Phenyl groups are able to inject electrons into the triazine ring and decrease the polarity and reactivity of alkynyl groups towards cyclotrimerization. Also, steric hindrance between bulky phenyl groups is a factor that can disfavor the cyclotrimerization.

To investigate the effects of steric hindrance, 2-chloro-4,6-methoxy-1,3,5-triazine (**7**) containing less bulky but strong electron donating substituents was used as a molecular model and its reaction with sodium acetylide was monitored by various spectroscopy methods (Fig. 2g). In this reaction, intermediate (**8**) was stable enough to be detected by ^{1}H NMR and ^{13}C NMR spectroscopy (Fig. 2h and i). However, neither NMR nor mass spectroscopy detected a signal for the product of cyclotrimerization (**9**). The ethynyl group in intermediate (**8**) was changed to a hydroxyl group upon reaction with water. Since methoxy groups were not too bulky but good electron donors, the absence of the product of cyclotrimerization indicates that the electronic effect is the dominating factor in this reaction. These model reactions showed that electron deficiency of the triazine ring plays a crucial role in the cyclotrimerization of ethynyl substituents. To further prove this statement, two additional more model reactions were performed. In the first reaction 2,4-dichloro-6-methoxy-1,3,5-triazine (**12**) with only one methoxy group was selected for the reaction with sodium acetylide (Fig. 3a). If the electron deficiency of triazine dominates the reactivity of ethynyl groups toward cyclotrimerization, this monomer should show higher tendency for cyclotrimerization than 2-chloro-4,6-methoxy-1,3,5-triazine (**7**). The product of reaction was evaluated by matrix-assisted laser desorption/ionization time-of-flight (MALDI-TOF) (Fig. 3b and c). Distinguished signals at 198n *m/z* and 75n *m/z* intervals, where n is a natural number, indicated structures (**14**) and (**15**) as repeating units of the product of reaction (**13**). Signals at 198n *m/z* intervals showed that the substitution of chlorine atoms of compound (**12**) is the first step of reaction and compound (**14**) is the intermediate of reaction. Also, repeating unit (**15**) at 75n *m/z* was corresponding to the benzene rings with three substitutions and proved the cyclotrimerization of ethynyl groups to the benzene rings. A comparison of this reaction with the similar reaction of compound (**7**) confirmed the huge effect of electron donating substituents on the outcome and pathway of the reaction. Based on these results, the electron deficiency of the triazine ring plays a key role in the cyclotrimerization of ethynyl substituents.

In the next step, we performed the reaction between cyanuric chloride and sodium acetylide in the presence of compound (**1**) (Fig. 3d). This reaction helped us to find the intermediate of reaction between sodium acetylide and cyanuric chloride. Also, we can understand whether the highly reactive intermediate (**17**) is able to force compound (**1**) towards cyclotrimerization or not. Due to the moderate dispersibility of the product in organic solvents, we were able to record its NMR and MALDI-TOF spectra. ^{1}H NMR spectra of compound (**16**) in $DMSO_{d6}$ showed a broad signal at 9–8.2 ppm corresponding to the aromatic protons of this compound (Fig. S9b). This signal was a further proof for the production of aromatic rings upon cyclotrimerization of alkynes. Also, a signal at 11.2 ppm together with a triplet signal at 7.25 ppm were assigned to O–H and N–H functional groups of sheet-like benzene-triazine heteroaromatic structures. The pathway for the creation of hydroxyl functional groups is explained in Fig. 2a and g. N–H functional groups were formed by tautomerization of triazine rings bearing hydroxyl groups, as verified by crystal structure of compound (**6**) (Fig. 2c). The disappearance and broadening of the signal at 11.2 ppm and 7.25 ppm upon D_2O addition was a further proof to be assigned to the O–H and N–H functional groups respectively (Fig. S9c). MALDI-TOF spectrum showed a repeating unit at 212n *m/z* intervals that belongs to intermediate (**17**). This result showed that production of PTrz goes through this intermediate (Fig. 3e).

After understanding the mechanism of reactions and analyzing the synthesized materials, the ability of PTrz18 for intercalation and storing various objects such as R6G and small gold nanoparticles (5 nm) was investigated (Fig. 4a). PTrz18 showed 43 % storage capacity for R6G (ESI page S25). The high capacity of PTrz18 for intercalation of R6G was assigned to its porous structure and highly accessible surface area for dye molecules. The redshift in the UV spectra of the intercalated R6G (PTrz/rh) was due to the local concentration of the dye inside the PTrz18 layers (Fig. 4b) [43]. Intercalation of R6G by PTrz18 gave rise to quenching at high concentrations but strong luminescence emission at low concentrations. Fig. 4c shows the luminescence of free and intercalated dye at various concentrations. At high concentration (100 μg ml^{-1}) neither free dye nor PTrz/rh showed any significant emission. Free dye displayed strong luminescence from 0.1 μg ml^{-1} concentrations. At high concentrations of free dye, the energy transfer to

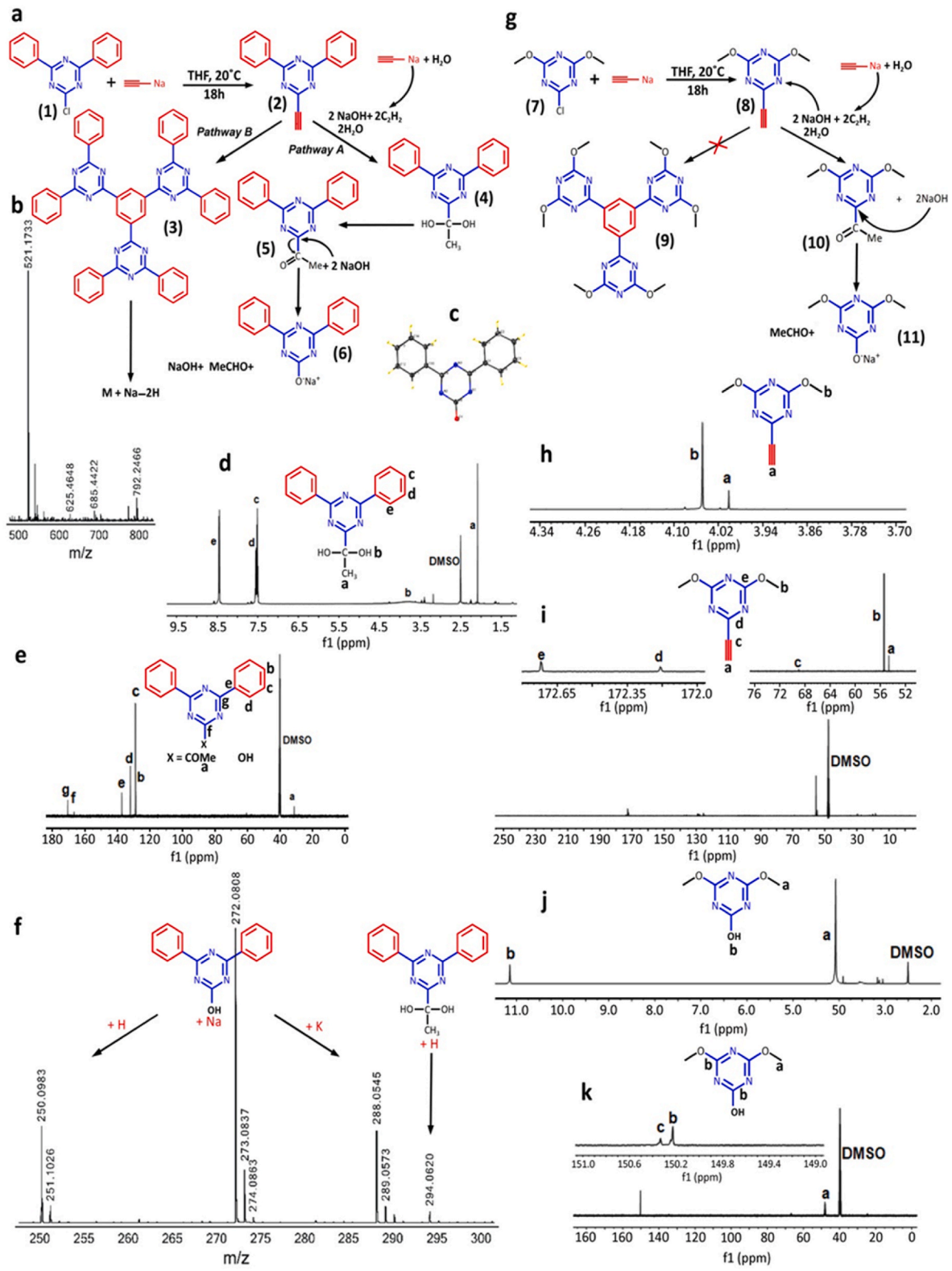

Fig. 2. Investigation of the mechanism of reaction between cyanuric chloride and sodium acetylide using model reactions. (a) Schematic representation of the mechanism of reaction between 2-chloro-4,6-diphenyl-1,3,5-triazine (**1**) and sodium acetylide. This reaction resulted in intermediate (**2**) which was changed to compounds (**6**) and (**3**) through reaction pathways **A** and **B**, respectively. (b) ESI mass spectrum of reaction mixture: *m/z* indicating compound (**3**) $C_{51}H_{33}N_9$ [M + Na–2H]: calcd: 792.28 and found: 792.24. (c) Single crystal XRD structure of compound (**6**). (d, e) ^{1}H and ^{13}C NMR spectra of intermediate (**5**) indicating a pathway for the creation methyl ketone and hydroxyl functional groups in the structure of PTrz. (f) ESI mass spectrum of reaction mixture: *m/z* displaying signals of compound (**4**) ($C_{17}H_{15}N_3O_2$ [M+H]: calcd: 294.12 and found: 294) and compound (**6**) ($C_{15}H_{11}N_3O$ [M+H], [M+Na] and [M+K]: calcd: 250.09, 272.08, 288.05 and found: 250.09, 272.08, 288.05, respectively). (g) Schematic representation of the mechanism of reaction between 2-chloro-4,6-methoxy-1,3,5-triazine (**7**) and sodium acetylide. Intermediate of this reaction (**8**) was detected by (h) ^{1}H NMR and (i) ^{13}C NMR spectra. (j, k) ^{1}H and ^{13}C NMR spectra of compound (**11**) respectively. Compound (**9**) was not detected.

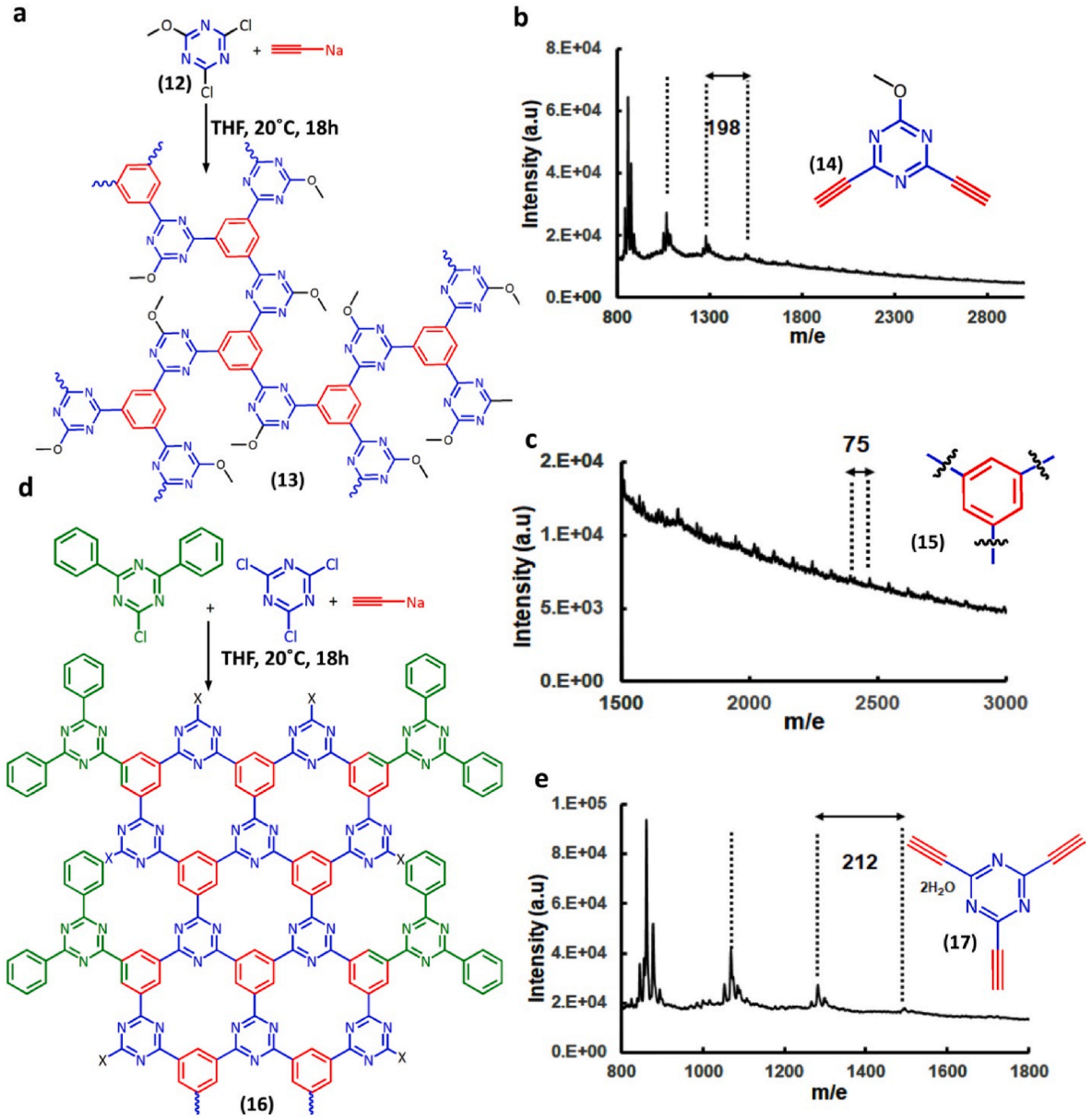

Fig. 3. Two model reactions to investigate the mechanism and intermediates of the synthesis of PTrz. (a) Schematic representation of the reaction between 2,4-dichloro-6-methoxy-1,3,5-triazine (**12**) and sodium acetylide. (b, c) MALDI-TOF spectra of compound (**13**) in methanol. Repeating units at 75n *m/z* intervals indicated the cyclotrimerization of ethynyl groups to benzene rings. (d) Schematic representation of the reaction between cyanuric chloride and sodium acetylide in the presence of compound (**1**). (e) MALDI-TOF spectrum of compound (**16**) in methanol, displaying intermediate (**17**) in 212n *m/z* intervals. This intermediate changed to PTrz upon cyclotrimerization.

aggregations was the reason of quenching [44]. It was more efficient for the intercalated dye, because the emitted fluorescence was absorbed by PTrz sheets dispersed in the medium. In contrast, a solution of PTrz/rh with only 0.1 μg ml^{-1} concentration showed strong emission. Considering a 43 % loading capacity, the dye content of PTrz/rh at this concentration was 89 pM. Confining dye molecules inside the layers of PTrz18 limited their interactions with other objects and lose non-radiative decay pathways. This was the reason for the strong emission of intercalated R6G at a picomolar range that cannot be observed for the free dye.

In order to explore whether the observed luminescence for PTrz/rh belongs to the intercalated R6G or dye molecules which are already released into the solution, the luminescence of PTrz/rh in the solid state was also investigated. In the solid state, encapsulated dyes were confined inside PTrz18 and did not leak to the medium. Free or physically absorbed dye was removed by washing the sheets that were fixed on the substrate. Any changes in the luminescence of dye can be linked to their local concentrations inside the sheets. From the PLE maps we learned that the strongest luminescence of the free and intercalated R6G is achieved by exciting at 520–540 nm. Therefore, free dye and PTrz/rh with 0.1 μg ml^{-1} concentration were dropped on silica, the solvent was evaporated at room temperature and then the samples were excited by laser 532 nm. A clear luminescence redshift, ~150 nm, together with a broadening of luminescence of the free dye in comparison with PTrz/rh showed that the dye aggregates upon evaporation of the solvent. Intercalation of dye molecules, however, inhibited their aggregation during solvent evaporation and PTrz/rh displayed an emission similar to the non-aggregated R6G (Fig. 4d). The maximum emission of intercalated dye at 560 nm with a shoulder at longer wavelengths was consistent with the PLE map of PTrz/rh in the solution

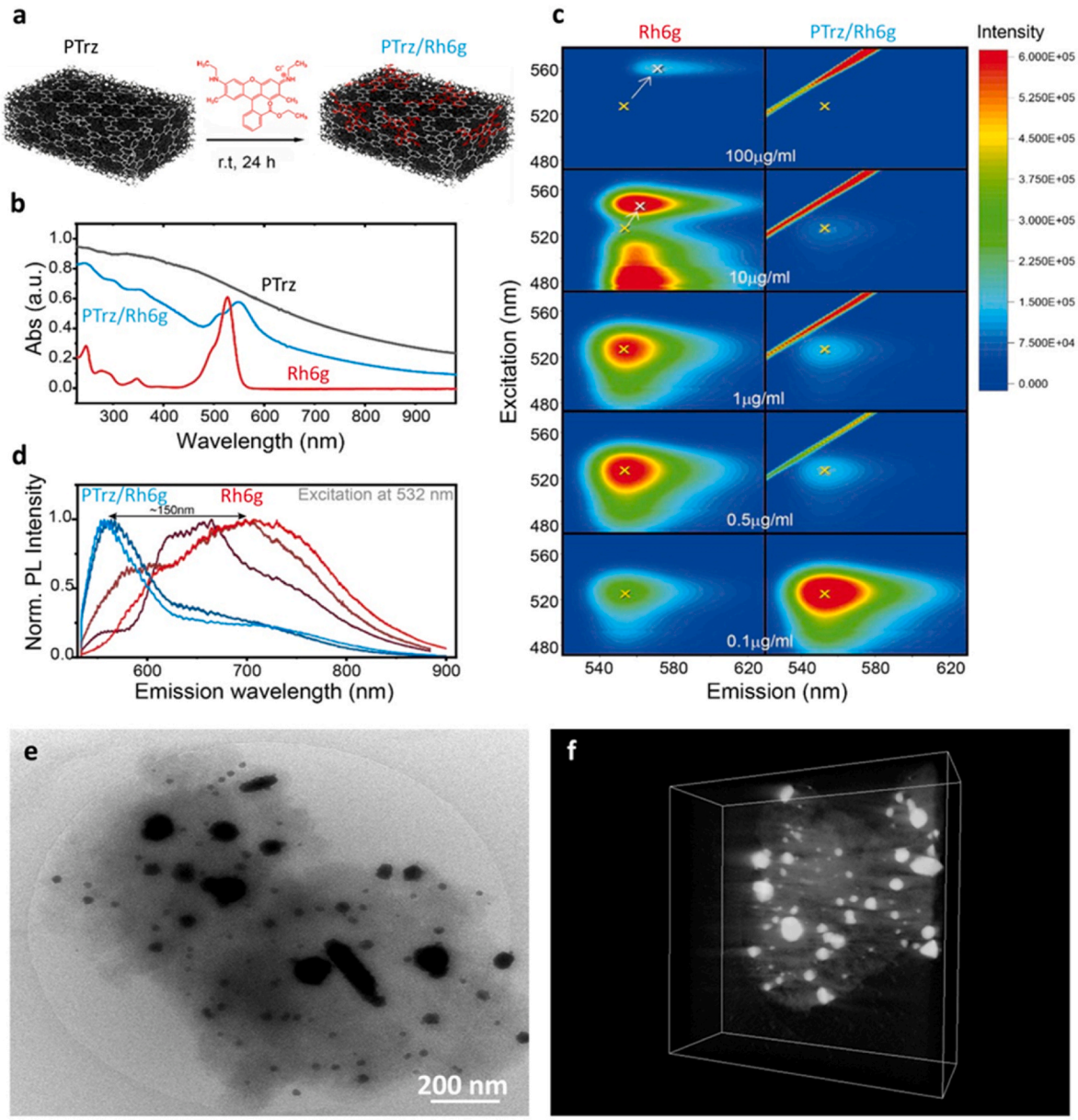

Fig. 4. Intercalation of Rhodamine 6G by PTrz18 in water and solid state. (a) Schematic representation of intercalation of R6G by nonexfoliated PTrz18. The porous structure of layers of PTrz18 allowed dye molecules to penetrate deep in this compound. (b) UV–vis spectra of PTrz, free R6G and PTrz/rh in water solution. (c) PLE maps of different concentrations of free R6G and PTrz/rh in water. (d) Luminescence of free R6G and PTrz/rh in the solid state. A water solution of samples with 0.1 μg ml^{-1} concentration was dropped on silica surface and dried under argon and excited by laser 532 nm. (e) Cryo-ET of PTrz18/intercalated gold nanoparticles. (f) Cryo-electron tomography of PTrz18/intercalated gold nanoparticles to elucidate the spatial structure under hydrated conditions without drying effects.

state. Therefore, the observed intense luminescence for the PTrz/rh in solution originates from the intercalated dye molecules.

The capability of the synthesized frameworks for the intercalation of bigger objects was also investigated. Spherical gold nanoparticles with 5 nm size were mixed with PTrz18, sonicated and stirred for several days at room temperature (Fig. S12a). UV spectra did not show a clear indication for the encapsulation of gold nanoparticles by PTrz18 (Fig. S10). To gain more information about the intercalation of gold nanoparticles, Cryo-ET was employed. According to the 3D reconstructed volume, only few gold nanoparticles penetrated the sheets, apparently only at the edges or through defects in the material (Fig. S12b). In the defect-free basal plane of two-dimensional nanomaterials no intercalated gold nanoparticles were detected, highlighting the site-selective penetration of nanoscale particles.

The size-selective permeability of PTrz18 was further verified via encapsulation and then reduction of $HAuCl_4$ molecules. PTrz18 was incubated with $HAuCl_4$ for several hours at room temperature and after purification subjected to reduction by trisodium citrate. Gold nanoparticles with different sizes were formed and trapped inside PTrz18, indicating permeability of this framework to small $HAuCl_4$ molecules and impermeability to big gold nanoparticles (Fig. 4e and f).

2.1. Dye adsorption performance of PTrz18

The permeability of PTrz18 to small molecules and impermeability to nanoparticles points to its potential application in water purification. Industrial dyes are one of the main sources of water contaminants and cause a severe threat to the human health and environmental safety [45]. Exploring new technologies and materials for the cost-effective and fast removing of these contaminants from water is important to

inhibit their adverse effects on the public health [46]. Covalent organic frameworks with porous structure and large number of heteroatoms are excellent candidates to remove these impurities from water efficiently [47,48]. The ability of PTrz18 for removing dyes including Methylene blue (MB), Malachite green (MG), Janus green (JC), Rhodamine B (RhB), Methyl orange (MO) and Congo red (CR) from water was investigated in different conditions (Fig. 5a).

PTrz18 (1 mg) removed 20 mg L^{-1} of MG and MB from water in 60 s upon sonication, indicating the high efficiency of this framework for the fast water purification (Fig. 5b). The combination of high adsorption capacity and fast water treatment is an advantage for PTrz18 superior to other systems in which one factor is improved with the cost of another [28,49,50].

In the next experiments, we didn't used sonication to make the

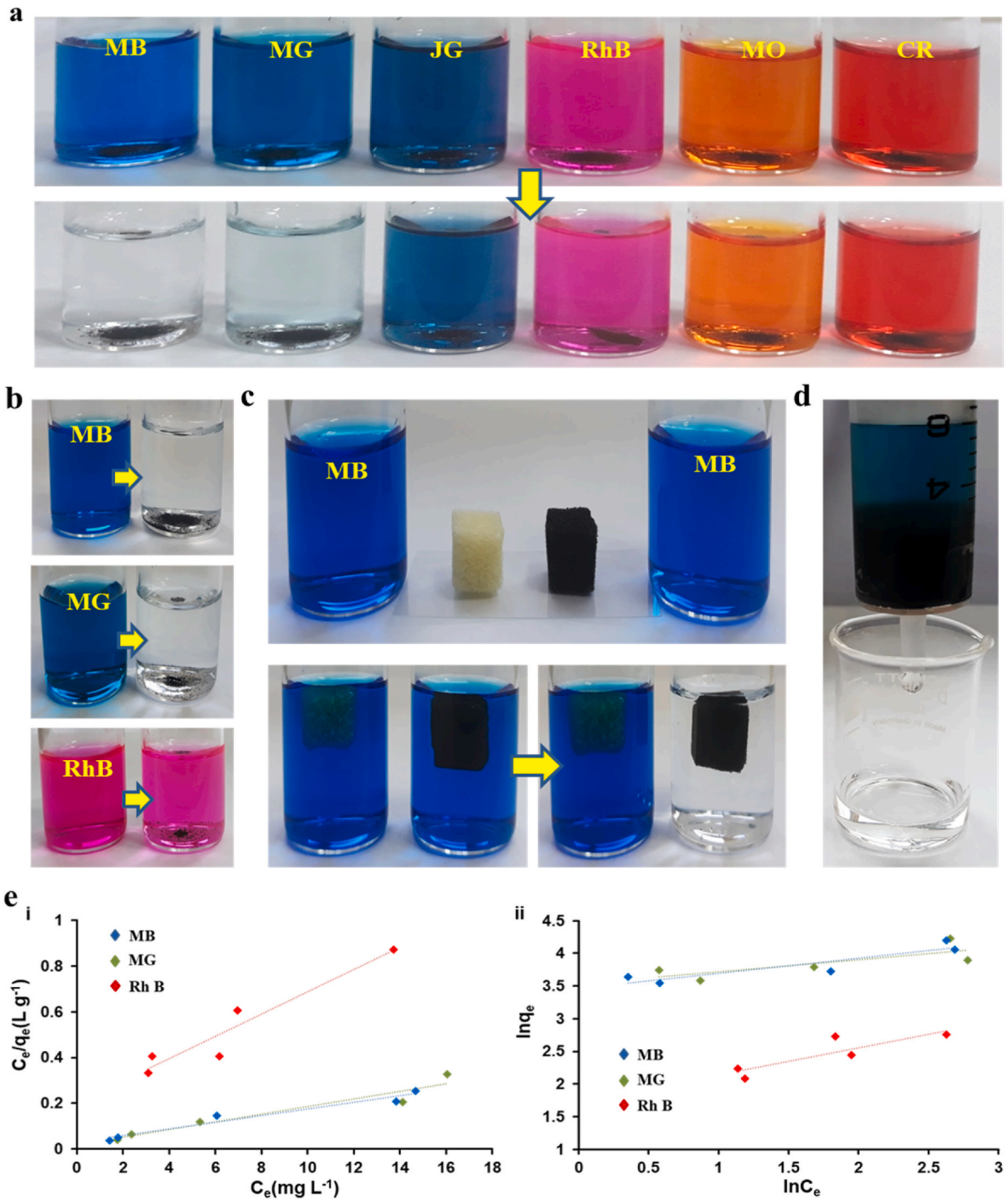

Fig. 5. (a) Different dyes incubated with PTrz18 after 1 min (upper row) and 30 min (bottom row). PTrz18 with the negative surface charge showed a high ability to remove positively charged dyes from water but less interactions with the neutral or negatively charged dyes. (b) Water solutions (20 mg L^{-1}) of MB, MG, and RhB before (left) and after (right) sonication with PTrz18 (1 mg). PTrz18 was added to dye solution and sonicated for 60 s at room temperature. (c) Complete removal of MB (20 mg L^{-1}) in 10 ml of water by cubic sponge-PTrz18 with 1cm × 1cm × 1 cm dimensions at room temperature without shaking. PTrz18 (20 mg) was deposited on a polyurethane sponge with the mentioned dimensions and used for the water purification. (d) The sponge-PTrz18 was fixed in a syringe and used as a filter to remove dyes from water. Filtering a water solution of MG (20 mg L^{-1}) by sponge-PTrz18 and complete removal of dye. (e) The adsorption mechanism models of the MB, MG and RhB by PTrz18. (i) Langmuir isotherm model, (ii) Freundlich isotherm model.

purification process easier and decrease the number of parameters influencing the mechanism of dye adsorption.

In order to study the mechanism of dye adsorption, PTrz18 (1 mg) was dispersed in 10 ml of dye solution (5–20 mg L^{-1}) and shaken continuously for 24 h under ambient condition (25 °C). The adsorption capacities were calculated using the following Formula (1):

$$q_t = \frac{(C_0 - C_e)V}{m} \quad (1)$$

Where q_e is the adsorption capacity of framework (mg g^{-1}), C_0 and C_e are the initial and final concentrations of dyes (mg L^{-1}), respectively, m is the mass of PTrz18 (g) and V is the volume of the dye solutions (L) [51].

The highest adsorption capacity was measured for Malachite green 185 mg g^{-1} and Methylene blue 205 mg g^{-1}. The fast and efficient dye exclusion by PTrz18 was assigned to its porous structure and high negative surface charge. Rhodamine B was also removed from water by PTrz18 efficiently but the adsorption capacity was lower than MB and MG (Table S10). A comparison study of adsorption capacity, for organic dyes are reported in Table S11. Also, the N_2 physisorption isotherms and the corresponding pore size distribution for PTrz18 indicates that PTrz18 has a narrow and well-defined distribution of micropores, with the specific surface area BET of 39.84 m^2 g^{-1}, pore volume of 0.23 cm^3 g^{-1} and average pore diameter of 9.54 nm, which belongs to type III isotherm according to IUPAC classification (Figs. S14a and S14b).

To make the water treatment easier and faster, PTrz18 (20 mg) was supported on polyurethane sponge with 1cm × 1cm × 1 cm dimensions and immersed in water containing methylene blue (20 mg L^{-1}) and malachite green (20 mg L^{-1}). The sponge-PTrz18 extracted dyes, completely, in 60 min by one time treatment, which is fast in comparison with the similar systems (Fig. 5c) [52–55]. Squeezing sponge pushed out the loaded dyes and made it ready for the next run of dye removal. The efficiency of sponge-PTrz18 after 18 runs extraction decreased 30 %, demonstrating the high renewability of this platform for water treatment. Moreover, sponge-PTrz18 with 2.5cm × 1 cm dimensions was fixed in a syringe and used as a filter to remove dyes from water (Fig. 5d). Water solutions of MG and MB (20 mg L^{-1}) were passed through the filter and cleaned water with less than 0.01 mg L^{-1} dye content was obtained. Owing to the fast dye removal, this filter is an excellent candidate for the cost-effective water purification.

To understand the mechanism of adsorption of MG, MB and RhB, the Langmuir and Freundlich isotherm models were studied using the following Eqs. (2) and (3):

$$\frac{C_e}{q_e} = \frac{1}{K_1 Q_m} + \frac{C_e}{Q_m} \quad (2)$$

$$\ln q_e = \ln K_f + \frac{1}{n} \ln C_e \quad (3)$$

where, Q_m was maximum adsorption capacity (mg g^{-1}), K_F and K_L were Freundlich and Langmuir constants, respectively and 1/n was Freundlich constant [56].

Correlation coefficient (R^2) of Langmuir isotherm model for adsorption of MB, MG and RhB by PTrz18 was bigger than that of Freundlich isotherm model and almost equal to unity, thus suitable for the prediction of adsorption capacity of this covalent organic framework (Fig. 5e). Fitting parameters for both models are summarized in Table S9. Based on Langmuir model, dyes were adsorbed homogenously on PTrz18 surface [57–60]. This highlights the role of electrostatic interactions, consisting repulsion between positively charged dyes but attraction with negatively charged PTrz18. The calculated adsorption capacities by Langmuir equation for MG, MB and RhB are shown in Table S9. The high adsorption capacity and fast uptake of MG and MB by PTrz18 was corresponding to the strong electrostatic attraction to the negative surface charge of framework [61,62]. In the case of RhB, the attraction force was deteriorated by negatively charged carboxylate group, leading to lower adsorption capacity in comparison with MG and MB. In the case of MO and CR, the permanent negative charge induce repulsion with PTrz18 and inhibit inertance of dyes into the backbone of this framework.

In order to explore the adsorption rate of dyes by PTRz18, the pseudo-first-order and pseudo-second-order kinetic models were studied for our systems [63], using Eqs. (4) and (5):

$$\log(q_e - q_t) = \log q_e - K_1 \frac{t}{2.303} \quad (4)$$

$$\frac{t}{q_t} = \frac{1}{K_2 q_e^2} + \frac{t}{q_e} \quad (5)$$

where K_1 and K_2 were the rate constants of pseudo-first-order (min^{-1}) and pseudo-second-order (g mg^{-1} min^{-1}) kinetics models, respectively and t was the adsorption time (min).

The pseudo-first-order and pseudo-second-order kinetic parameters including R^2, K_1, K_2, calculated q_e (q_{ecal}) and experimental q_e (q_{eexp}) are presented in Table S10. The kinetic data for adsorption of MG, MB and RhB by PTrz18 were fitted with pseudo-first-order model, indicating a physiosorption mechanism for the dye removal (Fig. 6a and b). This is confirmed by dependency of the kinetic of dye adsorption to the dye concentration but not, significantly, to PTrz18 concentration (Fig. 6) [55,64–67]. This result was counted for the reversible electrostatic and π-π interactions between surface of covalent organic framework and dyes. The reversible interactions are importance for the removing of excluded dyes from frameworks to be used for the next run of extractions. This is confirmed by repeating dye extraction by sponge-PTrz18. The reversible interactions between dyes and PTrz18 allowed 18 times adsorption and desorption cycles which impact purification process economically (Fig. 5c). Moreover, the adsorption efficiency of MB and MG in the five cycles indicating that PTrz18 can be used repeatedly for the removal of mentioned dyes (Fig. S14d).

The adsorption capacity versus time showed a concentration-dependent behavior. At low concentrations (5 mg L^{-1}), all dyes showed two phases but at higher concentrations (20 mg L^{-1}) three phases for MB and MG were realized. MB and MG with stronger electrostatic interactions, in comparison with RhB, were accumulated on the surface of PTrz18 at higher concentrations and caused a fast uptake by this framework (Fig. 6c).

3. Conclusion

Sheet-like benzene-triazine heteroaromatic structures with several micrometers lateral size were synthesized by the reaction between cyanuric chloride and sodium acetylide at room temperature. Due to their porosity, the synthesized material can be used for the size-selective molecular storage.

Ethynyl groups conjugated to a triazine ring are susceptible to catalyst-free cyclotrimerization at room temperature. This reaction overcomes challenges associated with the current cyclotrimerization of alkynes and opens up new ways for the construction of triazine covalent organic frameworks on gram scale. The size selective permeability of the synthesized frameworks provides a new strategy for the in-situ production and intercalation of nanoparticles. Due to their high porosity and negative surface charge, the synthesized frameworks are excellent candidates for the fast and efficient dye removal from water.

CRediT authorship contribution statement

Maryam Salahvarzi: Writing – original draft, Investigation. **Antonio Setaro:** Investigation. **Siamak Beyranvand:** Supervision. **Mohammad Nemati:** Formal analysis. **Georgy Gordeev:** Formal analysis. **Alphonse Fiebor:** Formal analysis. **Kai Ludwig:** Visualization, Formal analysis. **Reza Ghanbari:** Formal analysis. **Nima Nasiri:**

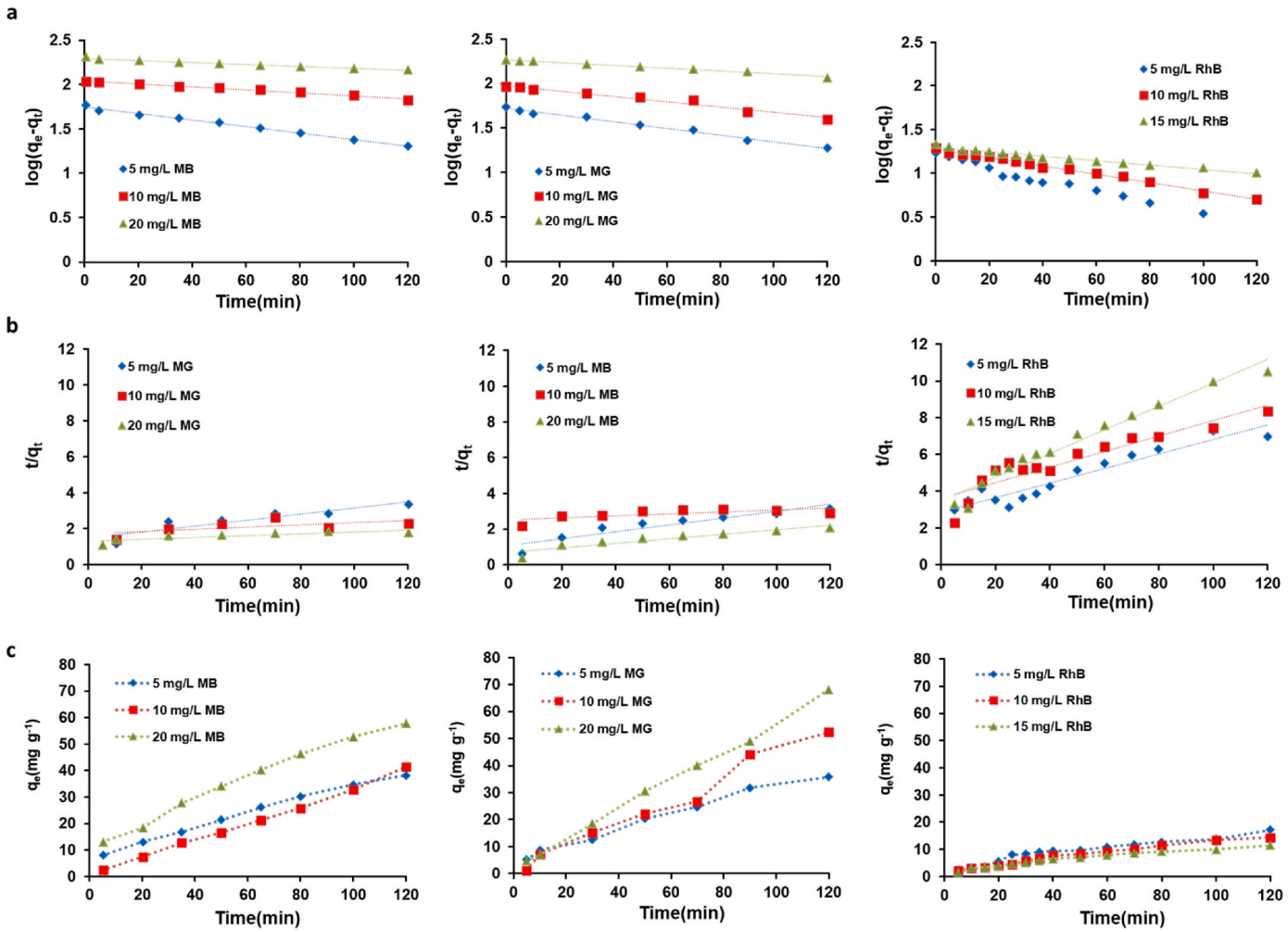

Fig. 6. The adsorption mechanism models of dyes by PTrz18. (a) Pseudo-first-order kinetics model. (b) Pseudo-second-order kinetics model. (c) Adsorption capacity model for the MB, MG and RhB.

Investigation, Formal analysis. **Vahid Ahmadi:** Formal analysis. **Manuela Weber:** Formal analysis. **Zahra Jamshidi:** Supervision. **Chong Cheng:** Writing – review & editing, Supervision. **Stephanie Reich:** Writing – review & editing, Conceptualization. **Mohsen Adeli:** Writing – review & editing, Conceptualization.

Declaration of competing interest

The authors declare that they have no known competing financial interests or personal relationships that could have appeared to influence the work reported in this paper.

Data availability

No data was used for the research described in the article.

Acknowledgement

The authors thank Andreas Schäfer for the solid-state NMR experiments. We acknowledge the European Research Council (ERC) with grant DarkSERS (772108) and Core Facility Biosupramol for Structural Research for the use of infrastructure. Also, authors would like to thank Iran Science Elites Federation and Iran National Science Foundation (Project Number 4001281) for the financial support.

Appendix A. Supplementary data

Supplementary data to this article can be found online at https://doi.org/10.1016/j.mtchem.2024.102155.

References

[1] Y. Li, W. Chen, W. Hao, Y. Li, L. Chen, Covalent organic frameworks constructed from flexible building blocks with high adsorption capacity for pollutants, ACS Appl. Nano Mater. 1 (9) (2018) 4756–4761.
[2] F. Yu, J.-H. Ciou, S. Chen, W.C. Poh, J. Chen, J. Chen, K. Haruethai, J. Lv, D. Gao, P.S. Lee, Ionic covalent organic framework based electrolyte for fast-response ultra-low voltage electrochemical actuators, Nat. Commun. 13 (1) (2022) 390.
[3] N.A. Khan, R. Zhang, X. Wang, L. Cao, C.S. Azad, C. Fan, J. Yuan, M. Long, H. Wu, M.A. Olson, Assembling covalent organic framework membranes via phase switching for ultrafast molecular transport, Nat. Commun. 13 (1) (2022) 3169.
[4] Q. Guan, L.-L. Zhou, Y.-B. Dong, Construction of covalent organic frameworks via multicomponent reactions, J. Am. Chem. Soc. 145 (2023) 1475.
[5] T. Ma, Y. Zhou, C.S. Diercks, J. Kwon, F. Gándara, H. Lyu, N. Hanikel, P. Pena-Sánchez, Y. Liu, N.J. Diercks, Catenated covalent organic frameworks constructed from polyhedra, Nature Synthesis (2023) 1–10.
[6] X. Li, K. Zhang, G. Wang, Y. Yuan, G. Zhan, T. Ghosh, W.P. Wong, F. Chen, H.-S. Xu, U. Mirsaidov, Constructing ambivalent imidazopyridinium-linked covalent organic frameworks, Nature Synthesis 1 (5) (2022) 382–392.
[7] Y. Xu, R.S. Sprick, N.J. Brownbill, F. Blanc, Q. Li, J.W. Ward, S. Ren, A.I. Cooper, Bottom-up wet-chemical synthesis of a two-dimensional porous carbon material with high supercapacitance using a cascade coupling/cyclization route, J. Mater. Chem. A 9 (6) (2021) 3303–3308.
[8] K. Wang, A. Osuka, J. Song, Pd-catalyzed cross coupling strategy for functional porphyrin arrays, ACS Cent. Sci. 6 (12) (2020) 2159–2178.
[9] H. Huang, F. Li, Y. Zhang, Y. Chen, Two-dimensional graphdiyne analogue Co-coordinated porphyrin covalent organic framework nanosheets as a stable

electrocatalyst for the oxygen evolution reaction, J. Mater. Chem. A 7 (10) (2019) 5575–5582.
[10] F. Hu, W. Hao, D. Mücke, Q. Pan, Z. Li, H. Qi, Y. Zhao, Highly efficient preparation of single-layer two-dimensional polymer obtained from single-crystal to single-crystal synthesis, J. Am. Chem. Soc. 143 (15) (2021) 5636–5642.
[11] C. Zhang, K. Hong, C. Pei, S. Zhou, W. Hu, A.S.K. Hashmi, X. Xu, Gold(I)-catalyzed intramolecular cyclization/intermolecular cycloaddition cascade as a fast track to polycarbocycles and mechanistic insights, Nat. Commun. 12 (1) (2021) 1182.
[12] F. Klappenberger, Y.-Q. Zhang, J. Björk, S. Klyatskaya, M. Ruben, J.V. Barth, On-surface synthesis of carbon-based scaffolds and nanomaterials using terminal alkynes, Accounts Chem. Res. 48 (7) (2015) 2140–2150.
[13] T. Shibata, K. Tsuchikama, Recent advances in enantioselective [2 + 2 + 2] cycloaddition, Org. Biomol. Chem. 6 (8) (2008) 1317–1323.
[14] J.H. Hardesty, J.B. Koerner, T.A. Albright, G.-Y. Lee, Theoretical study of the acetylene trimerization with CpCo, J. Am. Chem. Soc. 121 (25) (1999) 6055–6067.
[15] N. Agenet, V. Gandon, K.P.C. Vollhardt, M. Malacria, C. Aubert, Cobalt-catalyzed cyclotrimerization of alkynes: the answer to the puzzle of parallel reaction pathways, J. Am. Chem. Soc. 129 (28) (2007) 8860–8871.
[16] D.R. McAlister, J.E. Bercaw, R.G. Bergman, Parallel reaction pathways in the cobalt-catalyzed cyclotrimerization of acetylenes, J. Am. Chem. Soc. 99 (5) (1977) 1666–1668.
[17] K. Yamamoto, H. Nagae, H. Tsurugi, K. Mashima, Mechanistic understanding of alkyne cyclotrimerization on mononuclear and dinuclear scaffolds: [4 + 2] cycloaddition of the third alkyne onto metallacyclopentadienes and dimetallacyclopentadienes, Dalton Trans. 45 (43) (2016) 17072–17081.
[18] M.I. Lipschutz, T. Chantarojsiri, Y. Dong, T.D. Tilley, Synthesis, characterization, and alkyne trimerization catalysis of a heteroleptic two-coordinate FeI complex, J. Am. Chem. Soc. 137 (19) (2015) 6366–6372.
[19] X.Y. See, E.P. Beaumier, Z.W. Davis-Gilbert, P.L. Dunn, J.A. Larsen, A.J. Pearce, T. A. Wheeler, I.A. Tonks, Generation of TiII alkyne trimerization catalysts in the absence of strong metal reductants, Organometallics 36 (7) (2017) 1383–1390.
[20] G. Domínguez, J. Pérez-Castells, Recent advances in [2+2+2] cycloaddition reactions, Chem. Soc. Rev. 40 (7) (2011) 3430–3444.
[21] B.R. Galan, T. Rovis, Beyond reppe: building substituted arenes by [2+2+2] cycloadditions of alkynes, Angew. Chem. Int. Ed. 48 (16) (2009) 2830–2834.
[22] E. Pérez-Mayoral, V. Calvino-Casilda, E. Soriano, Metal-supported carbon-based materials: opportunities and challenges in the synthesis of valuable products, Catal. Sci. Technol. 6 (5) (2016) 1265–1291.
[23] R. Rao, C.L. Pint, A.E. Islam, R.S. Weatherup, S. Hofmann, E.R. Meshot, F. Wu, C. Zhou, N. Dee, P.B. Amama, Carbon nanotubes and related nanomaterials: critical advances and challenges for synthesis toward mainstream commercial applications, ACS Nano 12 (12) (2018) 11756–11784.
[24] A. Faghani, M.F. Gholami, M. Trunk, J. Muller, P. Pachfule, S. Vogl, I. Donskyi, M. Li, P. Nickl, J. Shao, Metal-assisted and solvent-mediated synthesis of two-dimensional triazine structures on Gram Scale, J. Am. Chem. Soc. 142 (30) (2020) 12976–12986.
[25] M. Hapke, Transition metal-free formal [2+2+2] cycloaddition reactions of alkynes, Tetrahedron Lett. 57 (51) (2016) 5719–5729.
[26] Q.-F. Zhou, F. Yang, Q.-X. Guo, S. Xue, DMAP-catalyzed benzannulation of ethyl propiolate with β-dicarbonyl moieties, Synlett 2007 (13) (2007) 2073–2076.
[27] A.P. Silvestri, J.S. Oakdale, Intermolecular cyclotrimerization of haloketoalkynes and internal alkynes: facile access to arenes and phthalides, Chem. Commun. 56 (87) (2020) 13417–13420.
[28] Z. Xia, Y. Zhao, S.B. Darling, Covalent organic frameworks for water treatment, Adv. Mater. Interfac. 8 (1) (2021) 2001507.
[29] Z. Wang, S. Zhang, Y. Chen, Z. Zhang, S. Ma, Covalent organic frameworks for separation applications, Chem. Soc. Rev. 49 (3) (2020) 708–735.
[30] H. Li, A.M. Evans, I. Castano, M.J. Strauss, W.R. Dichtel, J.-L. Bredas, Nucleation–elongation dynamics of two-dimensional covalent organic frameworks, J. Am. Chem. Soc. 142 (3) (2020) 1367–1374.
[31] M.S. Lohse, T. Bein, Covalent organic frameworks: structures, synthesis, and applications, Adv. Funct. Mater. 28 (33) (2018) 1705553.
[32] Y.-B. Zhang, J. Su, H. Furukawa, Y. Yun, F. Gándara, A. Duong, X. Zou, O.M. Yaghi, Single-crystal structure of a covalent organic framework, J. Am. Chem. Soc. 135 (44) (2013) 16336–16339.
[33] Z. Xiang, D. Cao, L. Huang, J. Shui, M. Wang, L. Dai, Nitrogen-doped holey graphitic carbon from 2D covalent organic polymers for oxygen reduction, Adv. Mater. 26 (20) (2014) 3315–3320.
[34] R. Cantu, S. Seetharaman, E.M. Babin, P.A. Karr, F. D'Souza, Paddle-wheel BODIPY–hexaoxatriphenylene conjugates: participation of redox-active hexaoxatriphenylene in excited-state charge separation to yield high-energy charge-separated states, J. Phys. Chem. 122 (15) (2018) 3780–3786.
[35] A. Faghani, M.F. Gholami, M. Trunk, J. Müller, P. Pachfule, S. Vogl, I. Donskyi, M. Li, P. Nickl, J. Shao, M.R.S. Huang, W.E.S. Unger, R. Arenal, C.T. Koch, B. Paulus, J.P. Rabe, A. Thomas, R. Haag, M. Adeli, Metal-assisted and solvent-mediated synthesis of two-dimensional triazine structures on gram scale, J. Am. Chem. Soc. 142 (30) (2020) 12976–12986.
[36] Q. Zhou, Y. Yang, J. Ni, Z. Li, Z. Zhang, Rapid recognition of isomers of monochlorobiphenyls at trace levels by surface-enhanced Raman scattering using Ag nanorods as a substrate, Nano Res. 3 (6) (2010) 423–428.
[37] K. Wang, D. Duan, M. Zhou, S. Li, T. Cui, B. Liu, J. Liu, B. Zou, G. Zou, Structural properties and halogen bonds of cyanuric chloride under high pressure, J. Phys. Chem. B 115 (16) (2011) 4639–4644.
[38] M. Sumathi, A. Prakasam, P.M. Anbarasan, Fabrication of hexagonal disc shaped nanoparticles g-C3N4/NiO heterostructured nanocomposites for efficient visible light photocatalytic performance, J. Cluster Sci. 30 (3) (2019) 757–766.
[39] P.V. Zinin, L.-C. Ming, S.K. Sharma, V.N. Khabashesku, X. Liu, S. Hong, S. Endo, T. Acosta, Ultraviolet and near-infrared Raman spectroscopy of graphitic C3N4 phase, Chem. Phys. Lett. 472 (1) (2009) 69–73.
[40] S. Kuecken, J. Schmidt, L. Zhi, A. Thomas, Conversion of amorphous polymer networks to covalent organic frameworks under ionothermal conditions: a facile synthesis route for covalent triazine frameworks, J. Mater. Chem. A 3 (48) (2015) 24422–24427.
[41] P. Katekomol, J. Roeser, M. Bojdys, J. Weber, A. Thomas, Covalent triazine frameworks prepared from 1,3,5-tricyanobenzene, Chem. Mater. 25 (9) (2013) 1542–1548.
[42] K. Wang, L.-M. Yang, X. Wang, L. Guo, G. Cheng, C. Zhang, S. Jin, B. Tan, A. Cooper, Covalent triazine frameworks via a low-temperature polycondensation approach, Angew. Chem. Int. Ed. 56 (45) (2017) 14149–14153.
[43] M. Lofaj, I. Valent, J. Bujdák, Mechanism of rhodamine 6G molecular aggregation in montmorillonite colloid, Cent. Eur. J. Chem. 11 (10) (2013) 1606–1619.
[44] K. Cyprych, Z. Kopczyńska, F. Kajzar, I. Rau, J. Mysliwiec, Tunable wavelength light emission and amplification in Rhodamine 6G aggregates, Adv. Device Mater. 1 (2) (2015) 69–73.
[45] R. Al-Tohamy, S.S. Ali, F. Li, K.M. Okasha, Y.A.-G. Mahmoud, T. Elsamahy, H. Jiao, Y. Fu, J. Sun, A critical review on the treatment of dye-containing wastewater: ecotoxicological and health concerns of textile dyes and possible remediation approaches for environmental safety, Ecotoxicol. Environ. Saf. 231 (2022) 113160.
[46] L. Chen, C. Zhou, L. Tan, W. Zhou, H. Shen, C. Lu, L. Dong, Enhancement of compatibility between covalent organic framework and polyamide membrane via an interfacial bridging method: toward highly efficient water purification, J. Membr. Sci. 656 (2022) 120590.
[47] C. Arqueros, F. Zamora, C. Montoro, A perspective on the application of covalent organic frameworks for detection and water treatment, Nanomaterials 11 (7) (2021) 1651.
[48] T.F. Machado, F.A. Santos, R.F. Pereira, V. de Zea Bermudez, A.J. Valente, M.E. S. Serra, D. Murtinho, β-ketoenamine covalent organic frameworks—effects of functionalization on pollutant adsorption, Polymers 14 (15) (2022) 3096.
[49] J. Wang, S. Zhuang, Covalent organic frameworks (COFs) for environmental applications, Coord. Chem. Rev. 400 (2019) 213046.
[50] A.R. Bagheri, N. Aramesh, Z. Liu, C. Chen, W. Shen, S. Tang, Recent advances in the application of covalent organic frameworks in extraction: a review, Crit. Rev. Anal. Chem. (2022) 1–34.
[51] Y. Li, C.-X. Yang, H.-L. Qian, X. Zhao, X.-P. Yan, Carboxyl-functionalized covalent organic frameworks for the adsorption and removal of triphenylmethane dyes, ACS Appl. Nano Mater. 2 (11) (2019) 7290–7298.
[52] X. Shi, D. Ma, F. Xu, Z. Zhang, Y. Wang, Table-salt enabled interface-confined synthesis of covalent organic framework (COF) nanosheets, Chem. Sci. 11 (4) (2020) 989–996.
[53] N. Basel, Q. Liu, L. Fan, Q. Wang, N. Xu, Y. Wan, Q. Dong, Z. Huang, T. Guo, Surface charge enhanced synthesis of TpEB-based covalent organic framework (COF) membrane for dye separation with three typical charge properties, Separ. Purif. Technol. 303 (2022) 122243.
[54] W.-L. Jin, W. Li, H.-X. Wang, X.-W. Liu, H.-X. Jiang, L.-N. Zhu, D.-M. Kong, Sponge-supported monolithic materials of porphyrin covalent organic frameworks for selective recognition, convenient removal and extraction of Cd2+, J. Environ. Chem. Eng. 10 (3) (2022) 107662.
[55] M. Zeng, M. Chen, D. Huang, S. Lei, X. Zhang, L. Wang, Z. Cheng, Engineered two-dimensional nanomaterials: an emerging paradigm for water purification and monitoring, Mater. Horiz. 8 (3) (2021) 758–802.
[56] S. Han, K. Liu, L. Hu, F. Teng, P. Yu, Y. Zhu, Superior adsorption and regenerable dye adsorbent based on flower-like molybdenum disulfide nanostructure, Sci. Rep. 7 (1) (2017) 43599.
[57] Y. Zhang, X. Hong, X.-M. Cao, X.-Q. Huang, B. Hu, S.-Y. Ding, H. Lin, Functional porous organic polymers with conjugated triaryl triazine as the core for superfast adsorption removal of organic dyes, ACS Appl. Mater. Interfaces 13 (5) (2021) 6359–6366.
[58] M.J. Pirouz, M.H. Amini, M.H. Beyki, Chromium-based covalent coordination nano-polymer: a promising dye elimination compound for water purification, Desalination Water Treat. 227 (2021) 360–369.
[59] L. Wang, Y. Tao, J. Wang, M. Tian, S. Liu, T. Quan, L. Yang, D. Wang, X. Li, D. Gao, A novel hydroxyl-riched covalent organic framework as an advanced adsorbent for the adsorption of anionic azo dyes, Anal. Chim. Acta 1227 (2022) 340329.
[60] S.-X. Xu, Z.-Q. Yao, Y.-H. Zhang, A covalent organic framework exhibiting amphiphilic selective adsorption toward ionic organic dyes tuned by pH value, Eur. Polym. J. 133 (2020) 109764.
[61] M. Najafi, S. Abednatanzi, P.G. Derakhshandeh, F. Mollarasouli, S. Bahrani, E. S. Behbahani, P. Van Der Voort, M. Ghaedi, Metal-organic and covalent organic frameworks for the remediation of aqueous dye solutions: adsorptive, catalytic and extractive processes, Coord. Chem. Rev. 454 (2022) 214332.
[62] Y. Song, J. Phipps, C. Zhu, S. Ma, Porous materials for water purification, Angew. Chem. 135 (11) (2023) e202216724.
[63] H. Zhang, X. Shi, J. Li, P. Kumar, B. Liu, Selective dye adsorption by zeolitic imidazolate framework-8 loaded UiO-66-NH2, Nanomaterials 9 (9) (2019) 1283.
[64] Y. Liu, Y. Cui, C. Zhang, J. Du, S. Wang, Y. Bai, Z. Liang, X. Song, Post-cationic modification of a pyrimidine-based conjugated microporous polymer for enhancing the removal performance of anionic dyes in water, Chem.–Eur. J. 24 (29) (2018) 7480–7488.
[65] A.R. Abdellah, H.N. Abdelhamid, A.-B.A. El-Adasy, A.A. Atalla, K.I. Aly, One-pot synthesis of hierarchical porous covalent organic frameworks and two-dimensional

nanomaterials for selective removal of anionic dyes, J. Environ. Chem. Eng. 8 (5) (2020) 104054.

[66] I. Mantasha, S. Hussain, M. Ahmad, M. Shahid, Two dimensional (2D) molecular frameworks for rapid and selective adsorption of hazardous aromatic dyes from aqueous phase, Separ. Purif. Technol. 238 (2020) 116413.

[67] J. Safaei, P. Xiong, G. Wang, Progress and prospects of two-dimensional materials for membrane-based water desalination, Materials Today Advances 8 (2020) 100108.